Experimental evidence of Xe incorporation in Schottky defects in UO_2

René Bes, Philippe Martin, Emerson Vathonne, Rémy Delorme, Catherine Sabathier, Michel Freyss, M. Bertolus, Pieter Glatzel

Experimental evidence of Xe incorporation in Schottky defects in UO2

René Bès, Philippe Martin, Emerson Vathonne, Rémy Delorme, Catherine Sabathier, Michel Freyss, Marjorie Bertolus, and Pieter Glatzel

Citation: Applied Physics Letters **106**, 114102 (2015); doi: 10.1063/1.4914300
View online: http://dx.doi.org/10.1063/1.4914300
View Table of Contents: http://scitation.aip.org/content/aip/journal/apl/106/11?ver=pdfcov
Published by the AIP Publishing

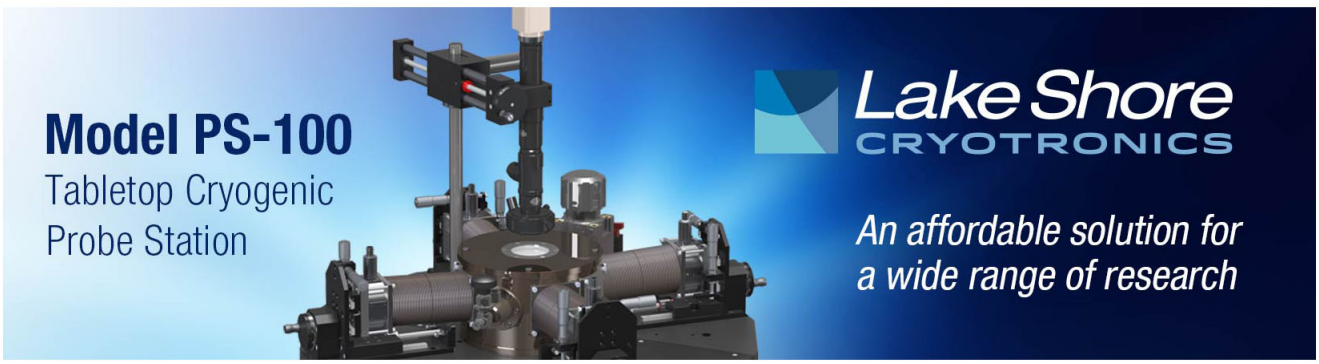

Experimental evidence of Xe incorporation in Schottky defects in UO_2

René Bès,[1,2,a)] Philippe Martin,[1,b)] Emerson Vathonne,[1] Rémy Delorme,[1] Catherine Sabathier,[1] Michel Freyss,[1] Marjorie Bertolus,[1] and Pieter Glatzel[3]
[1]*CEA, DEN, DEC, F-13108 Saint Paul Lez Durance Cedex, France*
[2]*Synchrotron SOLEIL, Ligne de Lumière MARS, L'Ormes des Merisiers, Saint Aubin, BP48, F-91192 Gif-sur-Yvette Cedex, France*
[3]*European Synchrotron Radiation Facility (ESRF), 6 Rue Jules Horowitz, BP 220, 38043 Grenoble Cedex 9, France*

(Received 5 January 2015; accepted 25 February 2015; published online 16 March 2015)

We report here the direct experimental observation of the preferential xenon incorporation site in uranium dioxide and analyse how its incorporation evolves with the annealing temperature. We show that High Energy Resolution Fluorescence Detection X-ray Absorption Near Edge Structure in combination with first-principles calculations enable a precise determination of the Xe incorporation site. Our finding provides important insight for the understanding and modeling of noble gases behavior in nuclear oxide fuel. © *2015 AIP Publishing LLC*.
[http://dx.doi.org/10.1063/1.4914300]

Rare gas behavior in materials has been at the heart of great research efforts for decades and cover many scientific domains such as geochemistry and planetary sciences,[1] medicine,[2] and nuclear applications.[3] Due to their insolubility in solids and their chemical inertness, noble gases can conveniently be used as a probe for chemical, physical, and structural changes in a wide range of materials as glasses,[4] semiconductors and metals,[5] as well as ceramics.[6] In particular, xenon can be used to investigate the microporosity distribution in materials.[7]

In the uranium dioxide nuclear fuel (UO_2), xenon is an abundant fission product. Due to their high insolubility in UO_2,[8] xenon atoms coalesce into bubbles, inducing swelling and degradation of the material properties.[9,10] The good understanding of the behavior of this gaseous fission product is mandatory for a safety-oriented control of the nuclear fuel evolution under nominal and transient conditions. One of the main difficulties to model xenon behavior in materials lies in predicting the ratio between xenon atoms isolated in the matrix and the ones forming nano-aggregates. The latter strongly influence the migration kinetics by trapping Xe atoms and affect their diffusion coefficient currently used in nuclear fuel performance codes.[11] Beyond the nuclear material interest, solid state chemistry modeling of gaseous incorporation in materials requires a complete evaluation of the pressure and the density of gas bubbles but also of the incorporation site of the isolated gas atom. Indeed, the knowledge of both the migration and coalescence of xenon as a function of *in operando* parameters, such as temperature, xenon concentration, or defect types, would increase our understanding of the crystal lattice dynamics separately from any chemistry.

A large amount of literature has been dedicated to experimental studies of xenon properties in nuclear fuels.[12–20] Most of the experimental studies however are limited to its precipitation to form bubbles and by the need of sufficient gas concentration to extract valuable experimental signal. Due to the difficulty to probe experimentally diluted impurities (less than 0.5 at. %) in a heavy matrix like UO_2, the xenon behavior (incorporation sites, pathways, and energetics of its migration) in UO_2 have been determined only using both density functional theory (DFT)[21–30] and empirical potentials.[11,26,29–38] The incorporation site and diffusion mechanisms have not unambiguously determined even if authors generally agree with the fact that due to steric constraints, vacancy trap sites are favored over interstitial sites. However, no clear experimental evidence has been provided yet. An efficient technique to obtain data about atomic ordering is X-ray Absorption Spectroscopy as it gives information about the local environment of one specific element diluted in a matrix. For example, by coupling Transmitted Electron Microscopy (TEM) observations and X-ray Absorption Spectroscopy (XAS) experiments at the xenon K-edge, the presence of highly pressurized (around 3 GPa) nanometer size bubbles in UO_2 has been recently demonstrated.[39,40] Most of the literature results have been obtained at relatively high concentration (some at. %), for which the formation of coarse bubbles was strongly expected. To ensure direct comparison with irradiated fuel, the concentration of Xe should have been 5 times less, but remains experimentally difficult to analyze because of the low signal over noise ratio.

In the past few years, the development of X-ray emission spectrometers on beamlines of synchrotron sources has allowed the study of highly diluted materials by High Energy Resolution Fluorescence Detection Spectroscopy (HERFD-XAS), which is a combination of XAS and X-ray Emission Spectroscopy (XES). This experimental approach increases drastically the signal over noise ratio, opening the door for the study of xenon at concentration encountered in irradiated nuclear fuels. However, the XAS interpretation is, in general, not straightforward. Spectra modeling remain a very useful tool to this aim. But XAS modeling codes require as input crystallographic data. This data can be derived from calculations such as electronic structure calculations (for instance, using DFT method).

[a)]rene.bes@cea.fr
[b)]philippe-m.martin@cea.fr

Samples were depleted UO_2 polycrystalline (^{235}U isotopic content of about 0.3% of total uranium) discs cut from sintered pellets (density about 98% of theoretical density). They were first polished and annealed 4 h at 1673 K in a reducing atmosphere of Ar + 5% H_2. They were then implanted with Xe ion at room temperature using the implantor at CSNSM laboratory (Orsay, France). The $^{129}Xe^{2+}$ implantation beam had an energy of 390 keV at normal incidence and the fluence was 1.7×10^{15} cm^{-2}. Considering a theoretical volumic mass of 10.96 g cm^{-3}, these conditions correspond to an ion projected depth of 71 nm (FWHM of 75 nm) as evaluated using the SRIM code.[41] The maximal concentration is about 0.37 at. %. Two samples were annealed under a reducing atmosphere (Ar + 5% H_2) during 12 h at 873 K and 4 h at 1673 K accordingly to the standard in pile and rapid power transient temperatures, respectively, measured in the intermediate pellet region of light water reactor irradiated fuel.

The Xe L_3-edge spectra were collected in fluorescence mode at the European Synchrotron Radiation Facility (ESRF, Grenoble, France) on the ID26 beamline using a wavelength dispersive crystal emission spectrometer.[42,43] Spectra were recorded in a continuous quick scan mode of both monochromator and undulator gap over the energy range. The spot size of the incident X-ray beam on the sample was 0.2×1 mm^2. Higher harmonics were rejected by three Si mirrors operating in total reflection. High energy resolution fluorescence detection was achieved by employing four spherically bent Si crystals (bending radius 1000 mm) with a (311) orientation in Rowland geometry. The incident energy was calibrated using a Ti foil (K-edge energy tabulated at 4966 eV). The emission spectrometer was tuned to the L_3M_5 ($L\alpha_1$ or $3d_{5/2}$–$2p_{3/2}$) emission line of Xe at 4109.6 eV. The paths of the incident and emitted X-rays through air were minimized in order to avoid undesirable absorption.

XAS spectra were systematically collected at 15 K using a He cryostat and at room temperature in order to be alternatively below and above the Xe melting point temperature of 110 K. The ATHENA software[44] was used for normalizing XANES spectra using linear functions for both pre-edge removal and post-edge normalization. The first maximum of the spectrum first energy derivative was used to determine the edge position E_0.

Figure 1 shows the HERFD-XANES spectra collected at room temperature and at 15 K.

The absorption spectra of the as-implanted and 873 K annealed samples are similar and characterized by a weak resonance at 4786 eV. Two broad intense peaks are also located around 4791 eV and 4794 eV, and are followed by a very broadened weak oscillation around 4808 eV. The annealing at 873 K causes only a slight evolution of the HERFD spectra compared to the as-implanted one. A 1 eV shift of the first broad peak at 4790 eV is measured in this case. As a consequence, small modifications of the geometry around xenon atoms are expected. Moreover, the thermal energy available during annealing at 873 K was insufficient to overcome the large diffusion barrier inducing Xe to be trapped. A strong resonance, the so-called white line, is present at 4786 eV on the HERFD spectra of the sample annealed

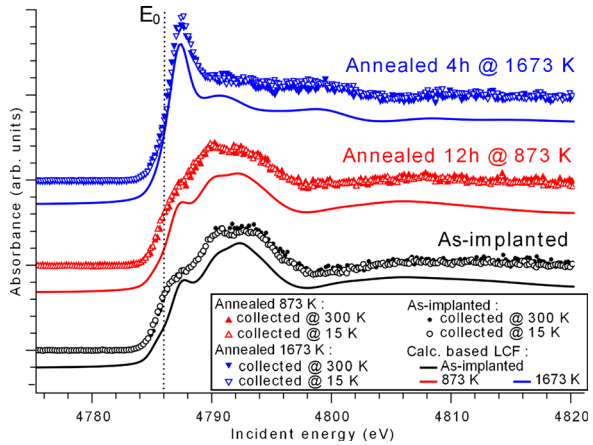

FIG. 1. HERFD-XANES spectra (symbols) and their best fit (line) using LCF at the Xe L_3 edge of as-implanted and annealed samples collected at room temperature (filled symbols) and at 15 K (open symbols). Dashed line indicates the energy position of the E_0 value. Spectra were vertically shifted for sake of clarity.

at 1673 K. Two slight oscillations with maxima located at 4791 eV and 4798 eV can be also observed on this spectra. At 1673 K, the width and shape of the absorption spectrum are very different compared to those observed on both the as-implanted and 873 K annealed samples. This is the sign of significant changes in the local environment of xenon atoms and a probable enhance mobility of these atoms. Finally, no significant change is noticed after cooling the sample from 300 K to 15 K. This indicates that Xe could not be in liquid or gaseous phase as the xenon melting point is 110 K. Consequently, the local environment of xenon atoms should consist of highly pressurized clusters and/or isolated atoms in the UO_2 fluorite structure.

To evaluate the local environment corresponding to these absorption spectra, XANES spectra were modeled using the FDMNES code.[45] These calculations were based on static atom supercells of hundred atoms and thermally induced disorder was not considered. The final states and resulting absorption cross sections were calculated using the muffin-tin approximation.[45] The impact of the muffin-tin approximation compared to finite difference method has been evaluated and can be neglected in our case. Due to the presence of heavy nuclei (U and Xe), spin-orbit effects were taken into account in the calculations. In HERFD-XANES, the width of the spectral features is no longer limited by the $2p_{3/2}$ (L_3 shell) core-hole lifetime (3.01 eV) but by the sharper $3d_{5/2}$ (M_5 shell) core-hole width (0.72 eV) in the final state.[43] The atomic coordinates used as input file for FDMNES calculations were derived from first-principles DFT + U optimized structure for Xe isolated atoms in UO_2 and determined using the $Fm\bar{3}m$ (225) crystallographic structure of solid xenon[46] for Xe bubbles.

The DFT calculations were performed in the periodic boundary conditions formalism using 96 atom supercell. The same parameters as those used in reference.[47] We have considered the incorporation of Xe in various positions in the UO_2 lattice such as octahedral interstitial (noted I_{Xe}), U and O mono-vacancies (noted V_U and V_O, respectively), and the Schottky defects. For the latter, the three possible orientations of the two oxygen divacancies, i.e., along the (100),

(110), and (111) directions, have been considered (noted as SD(100), SD(110), and SD(111), respectively).

The pressurized bubbles XANES spectra were modeled by using the cell parameter of Xe solid crystal compressed up to 15% (i.e., from 6.13 to 5.23 Å). In the following, they were noted as PB(X%), where X is the compression ratio of the cell parameter. The reference spectra, calculated with the structure optimized using DFT + U and with the Xe crystal structure, are reported in Figure 2. In order to take into account, the broadening due to disorder (from temperature and implantation process) and the energy resolution, all of the calculated spectra were convoluted with a Gaussian of 0.4 eV width before fitting.

The Xe crystal calculated spectra present a strong resonance at 4786 eV and two slight oscillations with maxima located around 4791 eV and 4798 eV. By increasing the pressure, the two oscillations are shifted to high energy. The calculated spectra of xenon incorporated in the UO_2 matrix have a weak resonance peak at 4786 eV and a broader, more intense feature around 4792 eV depending on the considered incorporation site. As the local environment of Xe atoms is quite similar for U vacancy and the three Schottky defects from the U sublattice point of view, the corresponding calculated spectra present strong similarities. Consequently, up to now, it has only been possible to discriminate the Xe interstitial site, the oxygen vacancy, and the xenon bubbles signals.

The fit of the experimental absorption spectra reported in Figure 1 was performed using Linear Combination Fitting (LCF) of the reference spectra, as implemented in the ATHENA software.

The best fits show that Xe is mainly located on a mix of uranium vacancy, Schottky defects, and pressurized bubbles, excluding oxygen vacancy, as reported in Table I.

The experimental spectra of the as-implanted and 873 K annealed samples are mainly composed of uranium vacancy and Schottky defects oriented along (100) and (111) directions. The concentration of the latter as well as the apparent trapping of Xe into an interstitial site of about 16% ± 2% is quite surprising as in our DFT + U calculations, these incorporation sites were strongly unfavored as compared to SD(100).[48] Such incorporations are probably the consequence of the structural disorder induced by the ion implantation process and not completely annealed at 873 K. Moreover, the high concentration of SD(111) can be considered as additional uranium vacancy percentage as the V_U and SD(111) spectra are very similar due to the identical geometry of first neighboring uranium atoms. Finally, the complement involves Xe weakly pressurized bubbles, for which the solid Xe cell parameter is at least compressed by about 5% (i.e., local density of Xe about 2.02×10^{22} Xe.cm^{-3}).

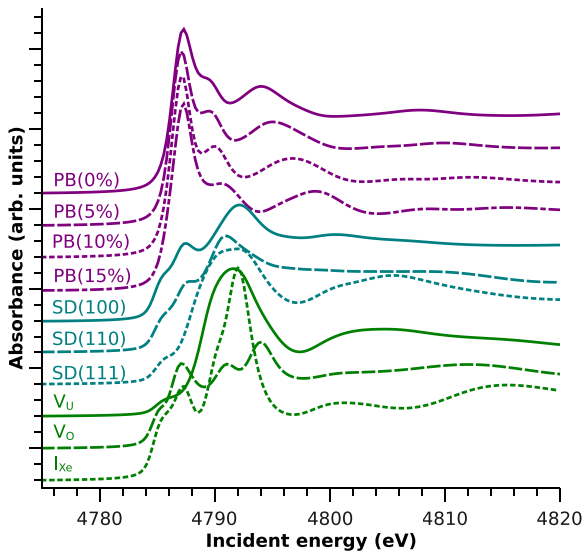

FIG. 2. Reference spectra calculated with FDMNES code[45] by using atomic position from DFT + U calculations and from solid Xe crystal properties.

TABLE I. Best fits derived value of the Xe local environment as a function of the samples. The values given here have been derived from the data collected at 15 K.

Local environment	As-implanted sample	Annealed 12 h at 873 K	Annealed 4 h at 1673 K
I_{Xe}	16^{+2}_{-2} %	16^{+1}_{-1} %	1^{+1}_{-1} %
V_U	9^{+4}_{-4} %	9^{+5}_{-5} %	2^{+2}_{-2} %
V_O	1^{+1}_{-1} %	1^{+1}_{-1} %	1^{+1}_{-1} %
SD(100)	17^{+7}_{-7} %	17^{+7}_{-7} %	23^{+6}_{-6} %
SD(110)	9^{+7}_{-7} %	9^{+8}_{-8} %	3^{+4}_{-3} %
SD(111)	18^{+5}_{-5} %	18^{+5}_{-5} %	2^{+3}_{-2} %
PB(0%)	20^{+10}_{-10} %	20^{+10}_{-10} %	5^{+8}_{-5} %
PB(5%)	12^{+9}_{-9} %	12^{+10}_{-10} %	12^{+11}_{-11} %
PB(10%)	5^{+5}_{-5} %	5^{+5}_{-5} %	5^{+4}_{-4} %
PB(15%)	4^{+4}_{-4} %	4^{+3}_{-4} %	60^{+6}_{-6} %
R-factor	0.0091	0.0084	0.0075

After annealing at 1673 K, Xe atoms diffuse and coalesce to form highly pressurized bubbles as illustrated by a solid Xe cell parameter compressed of about 15%. This compression corresponds to a local Xe density of about 2.80×10^{22} atoms cm^{-3}. The signal of these dense aggregates corresponds to about 60% of the experimental spectrum. The remaining percent of Xe has been found for 20% in low pressurized bubbles and for 23% in the Schottky defects with the two oxygen vacancies aligned along (100) direction. The latter is in agreement with our DFT + U calculations showing that this incorporation site is especially favored as compared to U vacancy and Schottky defects with oxygen vacancies aligned along (110) and (111) directions[48] in agreement with earlier studies.[49,50] Moreover, the concentrations of U vacancy and SD(111) tends to confirm that the local disorder is completely annealed at 1673 K.

We have thus presented here experimental evidence of the Xe incorporation in Schottky defects in UO_2 using an advanced approach to probe directly isolated atoms. We have shown that the experimental results of high energy resolution X-ray absorption spectroscopy at the Xe L_3-edge are directly comparable to electronic structure calculations. Further experiments and calculations are in progress to extend the discrimination of local environment in U vacancy and Schottky defects (from the U sublattice point of view). The method described in this paper can be performed on other species in materials and should be widely applied in the future.

Authors acknowledge the European Synchrotron Radiation Facility for providing beamtime, and also acknowledge Y. Joly for stimulating discussion about XANES simulation.

[1]C. Sanloup, B. C. Schmidt, G. Gudfinnsson, A. Dewaele, and M. Mezouar, Geochim. Cosmochim. Acta **75**, 6271 (2011).
[2]F. C. Marques, P. F. Barbieri, G. A. Viana, and D. S. da Silva, Appl. Surf. Sci. **275**, 156 (2013).
[3]C. Degueldre, M. Pouchon, M. Döbeli, K. Sickafus, K. Hojou, G. Ledergerber, and S. Abolhassani-Dadras, J. Nucl. Mater. **289**, 115 (2001).
[4]R. Bès, T. Sauvage, S. Peuget, J. Haussy, F. Chamssedine, E. Oliviero, T. Fares, and L. Vincent, J. Nucl. Mater. **443**, 544 (2013).
[5]H. J. Matzke, Thermochim. Acta **190**, 31 (1991).
[6]R. Bès, Y. Pipon, N. Millard-Pinard, S. Gavarini, and M. Freyss, Phys. Rev. B **87**, 024104 (2013).
[7]S. V. Filimonova, H. Knicker, W. Häusler, and I. Kögel-Knabner, Geoderma **122**, 25 (2004).
[8]G. Brillant, F. Gupta, and A. Pasturel, J. Nucl. Mater. **412**, 170 (2011).
[9]J. A. Turnbull, J. Nucl. Mater. **38**, 203 (1971).
[10]R. J. White, OECD Report HPR-368, 2008.
[11]K. Govers, S. Lemehov, and M. Verwerft, J. Nucl. Mater. **374**, 461 (2008).
[12]R. Lindner and H. J. Matzke, Z. Naturforsch., A: Phys. Sci. **14**, 582 (1959), available at: http://zfn.mpdl.mpg.de/data/Reihe_A/14/ZNA-1959-14a-0582_n.pdf.
[13]W. Miekeley and F. W. Felix, J. Nucl. Mater. **42**, 297 (1972).
[14]H. J. Matzke, Radiat. Eff. Defects Solids **53**, 219 (1980).
[15]H. J. Matzke, in *Diffusion Processes in Nuclear Materials*, edited by R. P. Agarwala (North-Holland, Amsterdam, 1992).
[16]G. Sattonnay, L. Vincent, F. Garrido, and L. Thomé, J. Nucl. Mater. **355**, 131 (2006).
[17]H. Kim, K. Park, Y. Yun, B. G. Kim, H. J. Ryu, K. C. Song, Y. S. Choo, and K. P. Hong, Ann. Nucl. Eng. **34**, 153 (2007).
[18]C. Sabathier, L. Vincent, P. Garcia, F. Garrido, G. Carlot, L. Thome, and C. Valot, Nucl. Instrum. Methods Phys. Res., Sect. B **266**, 3027 (2008).
[19]A. Michel, C. Sabathier, G. Carlot, O. Kaïtasov, S. Bouffard, P. Garcia, and C. Valot, Nucl. Instrum. Methods Phys. Res., Sect. B **272**, 218 (2012).
[20]B. Marchand, N. Moncoffre, Y. Pipon, C. Garnier, N. Bérerd, C. Delafoy, M. Fraczkiewicz, A. Perrat-Mabilon, L. Raimbault, P. Sainsot, and N. Toulhoat, Prog. Nucl. Energy **57**, 145 (2012).
[21]T. Petit, in *Fission Gas Behaviour in Water Reactor Fuels* (OECD, Cadarache, France, 2002), p. 269.
[22]M. Freyss, N. Vergnet, and T. Petit, J. Nucl. Mater. **352**, 144 (2006).
[23]Y. Yun, H. Kim, and K. Park, J. Nucl. Mater. **378**, 40 (2008).
[24]P. V. Nerikar, X.-Y. Liu, B. P. Uberuaga, C. R. Stanek, S. R. Phillpot, and S. B. Sinnot, J. Phys.: Condens. Matter. **21**, 435602 (2009).
[25]F. Zhou and V. Ozolins, Phys. Rev. B **80**, 125127 (2009).
[26]P. Tiwary, A. van de Walle, B. Jeon, and N. Grønbech-Jensen, Phys. Rev. B **83**, 094104 (2011).
[27]B. E. Hanken, C. R. Stanek, N. Grønbech-Jensen, and M. Asta, Phys. Rev. B **84**, 085131 (2011).
[28]D. A. Andersson, B. P. Uberuaga, P. V. Nerikar, C. Unal, and C. R. Stanek, Phys. Rev. B **84**, 054105 (2011).
[29]X.-Y. Liu, B. P. Uberuaga, D. A. Andersson, C. R. Stanek, and K. E. Sickafus, Appl. Phys. Lett. **98**, 151902 (2011).
[30]A. E. Thompson and C. Wolverton, Phys. Rev. B **87**, 104105 (2013).
[31]C. R. A. Catlow and R. W. Grimes, J. Nucl. Mater. **165**, 313 (1989).
[32]R. W. Grimes, in *Fundamental Aspects of Inert Gases in Solids*, edited by S. E. Donnelly and H. J. Evans (Springer, New York, 1990), p. 415.
[33]R. G. J. Ball and R. W. Grimes, J. Nucl. Mater. **188**, 216 (1992).
[34]S. Nicoll, H. J. Matzke, and C. R. A. Catlow, J. Nucl. Mater. **226**, 51 (1995).
[35]C. R. Stanek and R. W. Grimes, J. Nucl. Mater. **282**, 265 (2000).
[36]K. Govers, S. Lemehov, M. Hou, and M. Verwerft, J. Nucl. Mater. **376**, 66 (2008).
[37]B. Jeon, M. Asta, S. M. Valone, and N. Grønbech-Jensen, Nucl. Instrum. Methods Phys. Res., Sect. B **268**, 2688 (2010).
[38]A. Jelea, R. J.-M. Pellenq, and F. Ribeiro, J. Nucl. Mater. **444**, 153 (2014).
[39]P. Garcia, P. Martin, G. Carlot, E. Castelier, M. Ripert, C. Sabathier, C. Valot, F. D'Acapito, J.-L. Hazemann, O. Proux, and V. Nassif, J. Nucl. Mater. **352**, 136 (2006).
[40]P. Martin, P. Garcia, G. Carlot, C. Sabathier, C. Valot, V. Nassif, O. Proux, and J.-L. Hazemann, Nucl. Instrum. Methods Phys. Res., Sect. B **266**, 2887 (2008).
[41]J. F. Ziegler, J. P. Biersack, and M. D. Ziegler, *The Stopping and Range of Ions in Matter* (2008), see www.SRIM.org.
[42]C. Gauthier, V. A. Solé, R. Signorato, J. Goulon, and E. Moguiline, J. Synchrotron Radiat. **6**, 164 (1999).
[43]P. Glatzel, T.-C. Weng, K. Kvashnina, J. Swarbrick, M. Sikora, E. Gallo, N. Smolentsev, and R. A. Mori, J. Electron. Spectrosc. Relat. Phenom. **188**, 17 (2013).
[44]B. Ravel and M. Newville, J. Synchrotron Radiat. **12**, 537 (2005).
[45]O. Bunau and Y. Joly, J. Phys.: Condens. Matter **21**, 345501 (2009).
[46]D. Sears and H. Klug, J. Chem. Phys. **37**(2), 3002 (1962).
[47]E. Vathonne, J. Wiktor, M. Freyss, G. Jomard, and M. Bertolus, J. Phys.: Condens. Matter **26**, 325501 (2014).
[48]E. Vathonne "Étude par calculs de structure électronique des dégâts d'irradiation dans le combustible nucléaire UO2 : comportement des défauts ponctuels et gaz de fission," Ph.D. Thesis, Aix-Marseille Université (2014).
[49]A. E. Thompson and C. Wolverton, Phys. Rev. B **84**, 134111 (2011).
[50]M. Bertolus, M. Freyss, B. Dorado, G. Martin, K. Hoang, S. Maillard, R. Skorek, Ph. Garcia, C. Valot, A. Chartier, L. Van Brutzel, P. Fossati, R. W. Grimes, D. C. Parfitt, C. L. Bishop, S. T. Murphy, M. J. D. Rushton, D. Staicu, E. Yakub, S. Nichenko, M. Krack, F. Devynck, R. Ngayam-Happy, K. Govers, C. S. Deo, and R. K. Behera, J. Nucl. Mater. (published online).